天体計測学特論 I
Observational Astronomy I

Lecture 05:
Detecting light
Detectors in visible/NIR wavelength

Detecting photons

- External photoelectric effect (外部光電効果) : electron expelled from a material: phototube, photomultiplier tube (光電子倍増管), etc.

Hamamatsu photonics

- Internal photoelectric effect (内部光電効果) : electron excited to conduction band inside material (conduction electron) : CCD, etc.

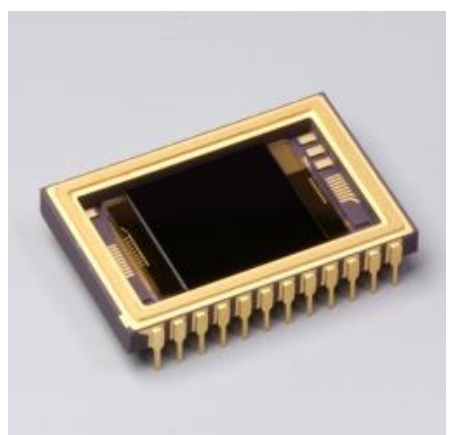

Hamamatsu photonics

Photon detection basics (I)

- Electron promoted from the valence energy band (価電子帯) (band gap) → to the conduction energy band (伝導帯)
- Band gap in Si corresponds to 1.1um. Si is transparent to IR light.
- (Smaller band gap is necessary to detect near IR photon).

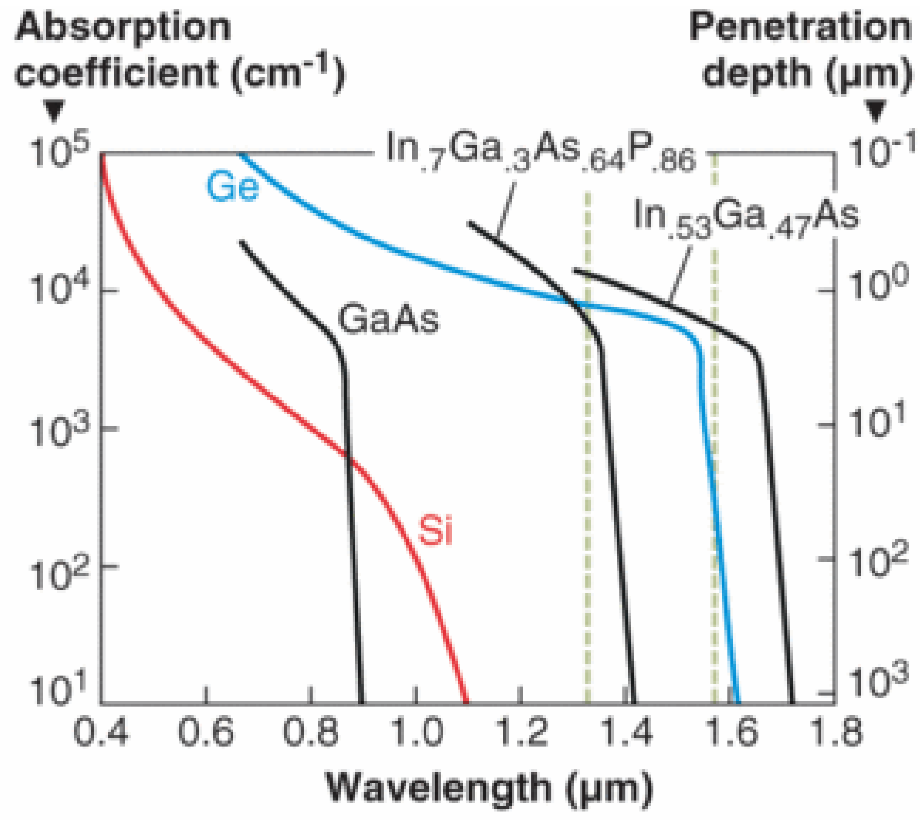

www.laserfocusworld.com

Photon detection basics (II)

- InSb (indium antimony) band gap 0.22 eV at 77K = lambda_c~5.6um
- HgCdTe (mercury cadmium tellurium)

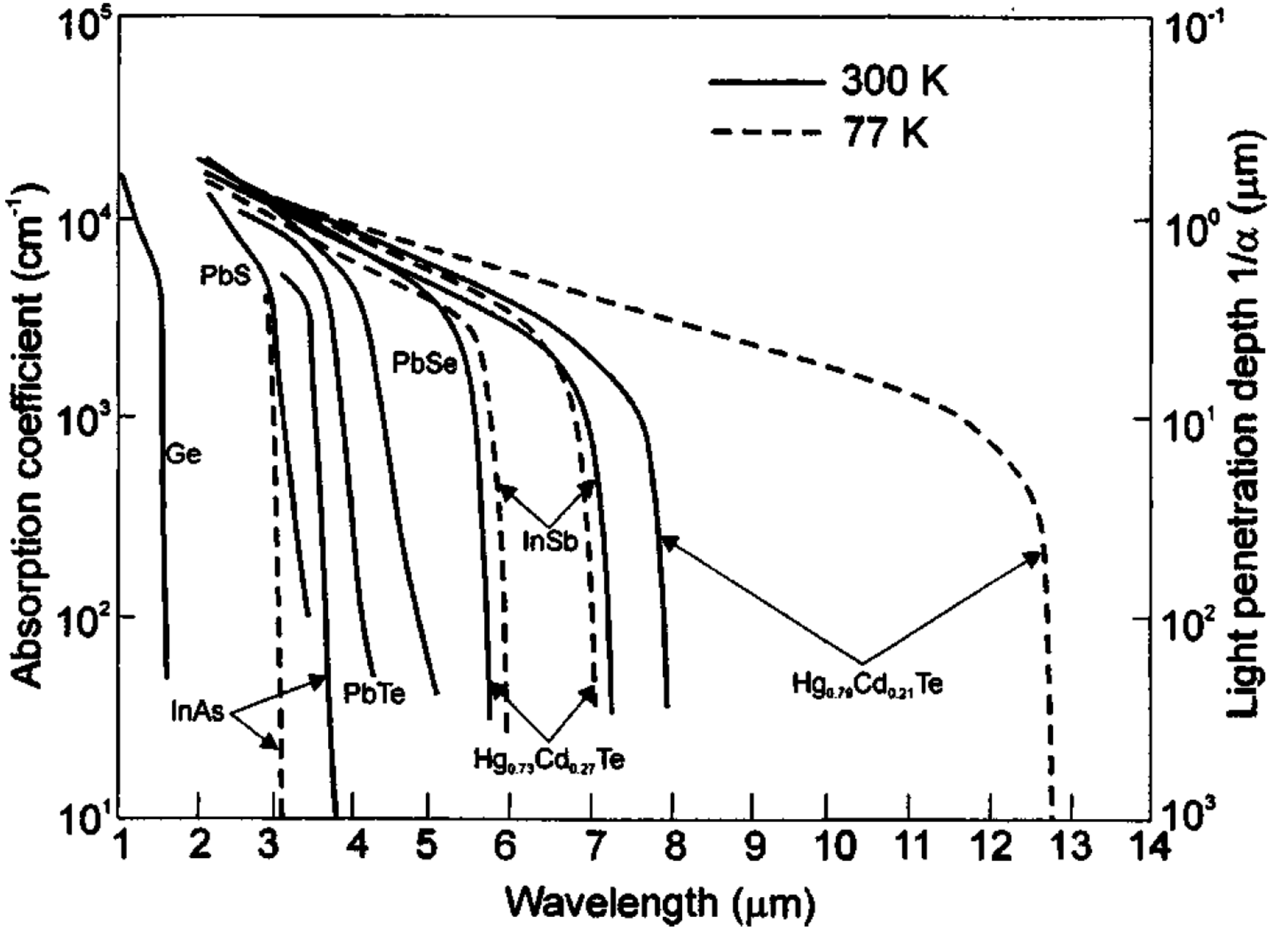

Rogalski 2003

Photon detection basics (III)

- $Hg_{1-x}Cd_xTe$: wavelength range can be adjustable by changing the composition.

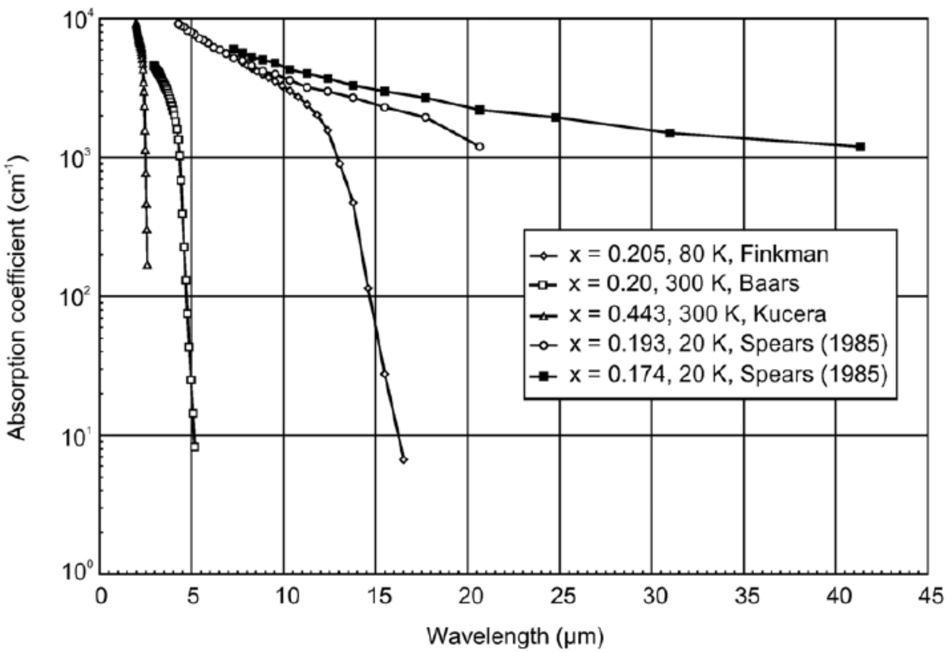

Figure 2. Optical absorption coefficient data for several $Hg_{1-x}Cd_xTe$ alloy compositions, for photon energies near the fundamental absorption edge, plotted versus wavelength (after [2]).

Table 1. Summary of the material properties for the $Hg_{1-x}Cd_xTe$ ternary alloy, listed for the binary components HgTe and CdTe, and for several technologically important alloy compositions (after [2]).

Property	HgTe	$Hg_{1-x}Cd_xTe$						CdTe
x	0	0.194	0.205	0.225	0.31	0.44	0.62	1.0
a (Å)	6.461	6.464	6.464	6.464	6.465	6.468	6.472	6.481
	77 K	77 K	77 K	77 K	140 K	200 K	250 K	300 K
E_g (eV)	−0.261	0.073	0.091	0.123	0.272	0.474	0.749	1.490
λ_c (μm)	—	16.9	13.6	10.1	4.6	2.6	1.7	0.8
n_i (cm^{-3})	—	1.9×10^{14}	5.8×10^{13}	6.3×10^{12}	3.7×10^{12}	7.1×10^{11}	3.1×10^{10}	4.1×10^{5}
m_c/m_0	—	0.006	0.007	0.010	0.021	0.035	0.053	0.102
g_c	—	−150	−118	−84	−33	−15	−7	−1.2
$\varepsilon_s/\varepsilon_0$	20.0	18.2	18.1	17.9	17.1	15.9	14.2	10.6
$\varepsilon_\infty/\varepsilon_0$	14.4	12.8	12.7	12.5	11.9	10.8	9.3	6.2
n_r	3.79	3.58	3.57	3.54	3.44	3.29	3.06	2.50
μ_e ($cm^2 V^{-1} s^{-1}$)	—	4.5×10^5	3.0×10^5	1.0×10^5	—	—	—	—
μ_{hh} ($cm^2 V^{-1} s^{-1}$)	—	450	450	450	—	—	—	—
$b = \mu_e/\mu_\eta$	—	1000	667	222	—	—	—	—
τ_R (μs)	—	16.5	13.9	10.4	11.3	11.2	10.6	2
τ_{A1} (μs)	—	0.45	0.85	1.8	39.6	453	4.75×10^3	
$\tau_{typical}$ (μs)	—	0.4	0.8	1	7	—	—	—
E_p (eV)				19				
Δ (eV)				0.93				
m_{hh}/m_0				0.40–0.53				
ΔE_v (eV)				0.35–0.55				

Rogalski 2005

Photon detection basics (IV)

Table 6.3. *Maximum usable wavelengths for several common detector materials*

Material	Temp (K)	λ_{cutoff}
Si	295	1.11
Ge	295	1.85
InSb	77	5.4
HgCdTe[1]	77	2.5
Si:As	5	23
Si:As[2] (BIB)[4]	5	30
Si:Sb		36
Si:Sb[2] (BIB)[4]	5	40
Si:Ga[3]	10	17.5
Ge:Ga	–	115
Ge:Ga (stressed)	–	>200

Notes: 1. By changing the detailed composition, the bandgap of HgCdTe can be adjusted over a considerable range. The figures shown here are for the NICMOS chips. 2. This is from Stapelbroek et al. (1995). 3. This is from Lucas et al. (1995). 4. See section 6.4.3.

Glass 1999

Storing electrons in semiconductor material

- Photo conductors
  - Current with photo absorption
  - A photo electron can disappear by recombination with a hole in the material.

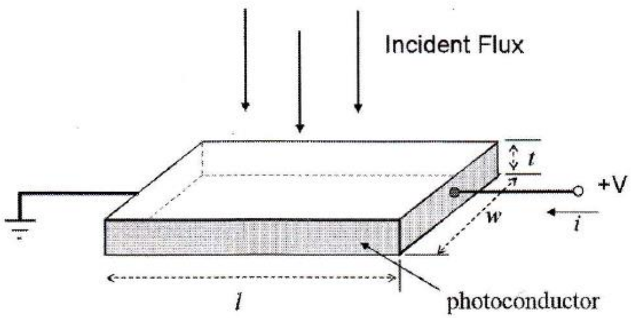

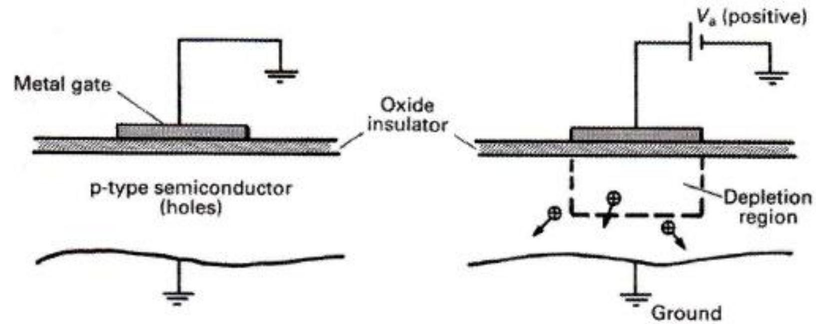

McLean 2008

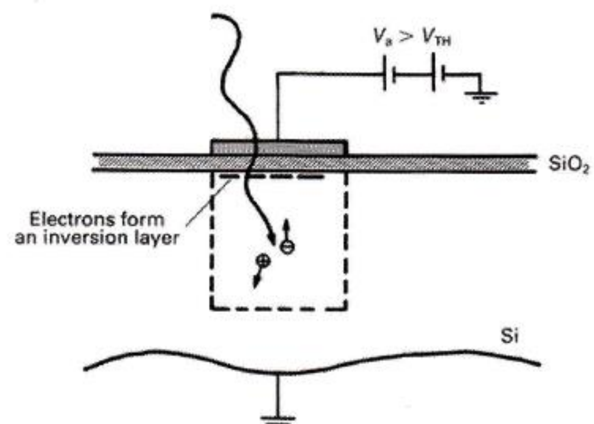

Storing electrons in semiconductor material

- Photo diode
  - Diode : p-type = more holes + n-type = more electrons
  - Use pn junction to make depletion layer, region without a carrier
  - Created electron-hole pair will be separated by the electric field, and the electron will be stored in the electron rich n-type region

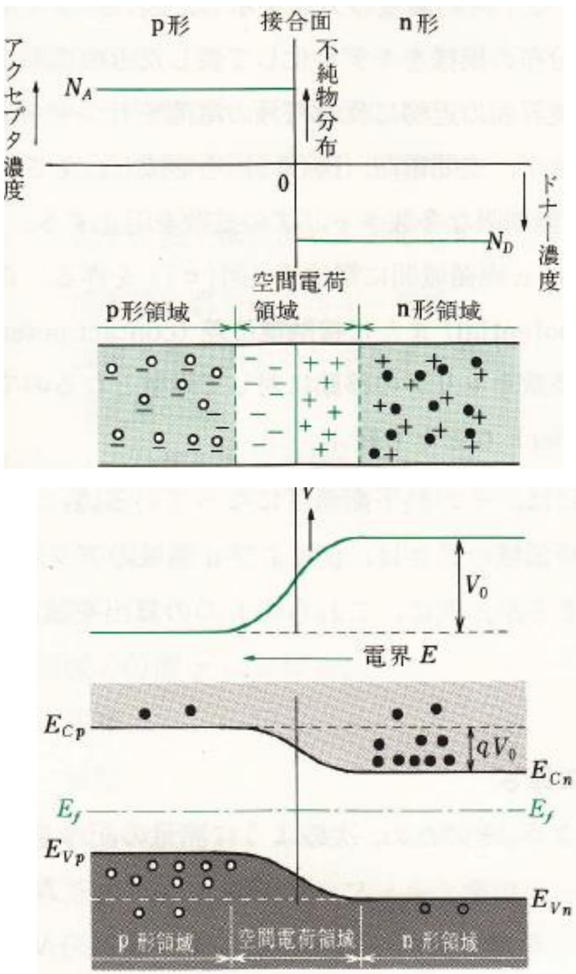

Shinkai 1986

insulator

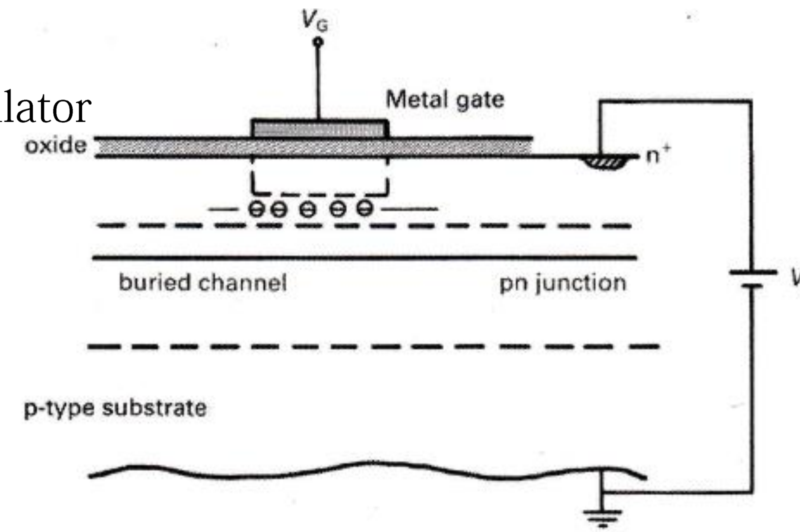

McLean 2008

Electron transfer in CCD (I)

- Si : semiconductor (low conductivity)
- Electron creation : (1) photo-absorption, (2) spontaneous thermal process (← noise : dark current)

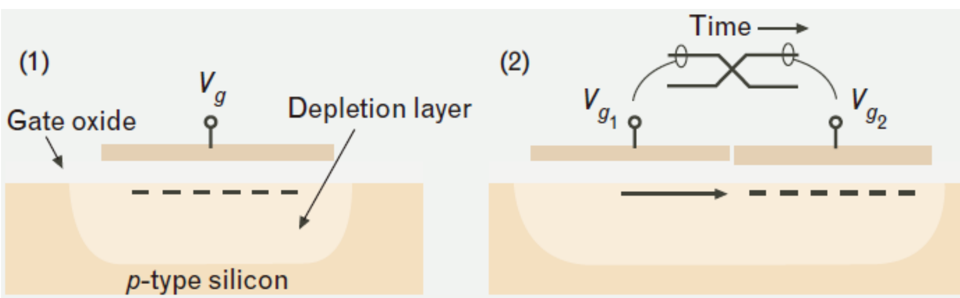

FIGURE A. (1) Cross section of a metal-oxide semiconductor (MOS) capacitor consisting of a biased gate electrode, an oxide layer, and a *p*-type silicon substrate. With the gate biased positive, a packet of electrons can be collected and held at the silicon/oxide interface. (2) With two closely spaced MOS capacitors, a packet of electrons can be exchanged between them by using a sequence of voltage steps on the two gates.

Burk et al. 2007

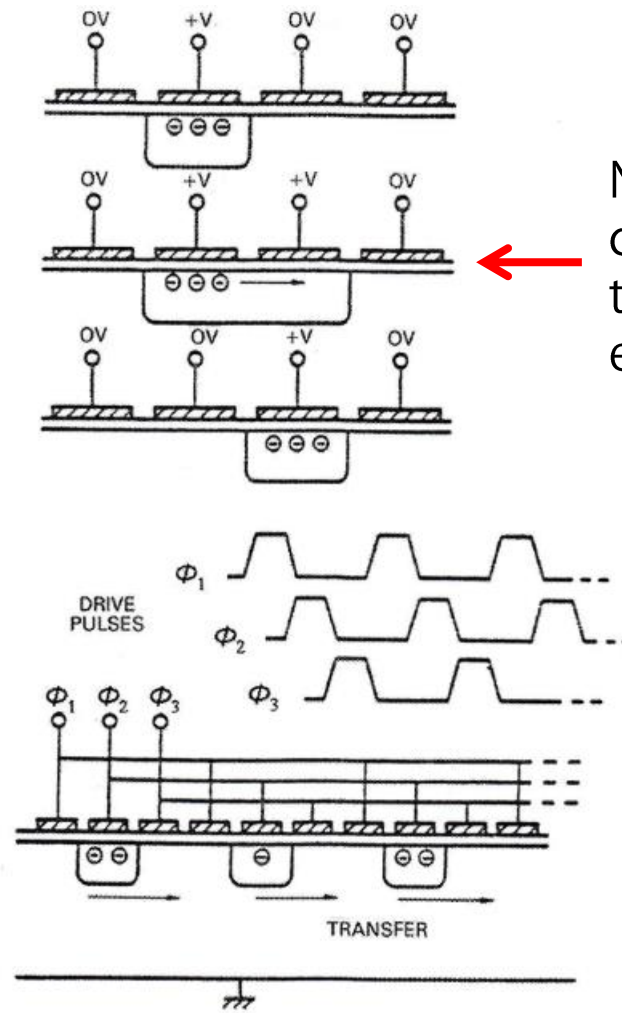

Noise: charge transfer efficiency ←

McLean 2008

Figure 7.7. The basic charge-coupling principle in a three-phase CCD and the associated timing or clock pattern.

Electron transfer in CCD (II)

- Real structure of a three-phase CCD

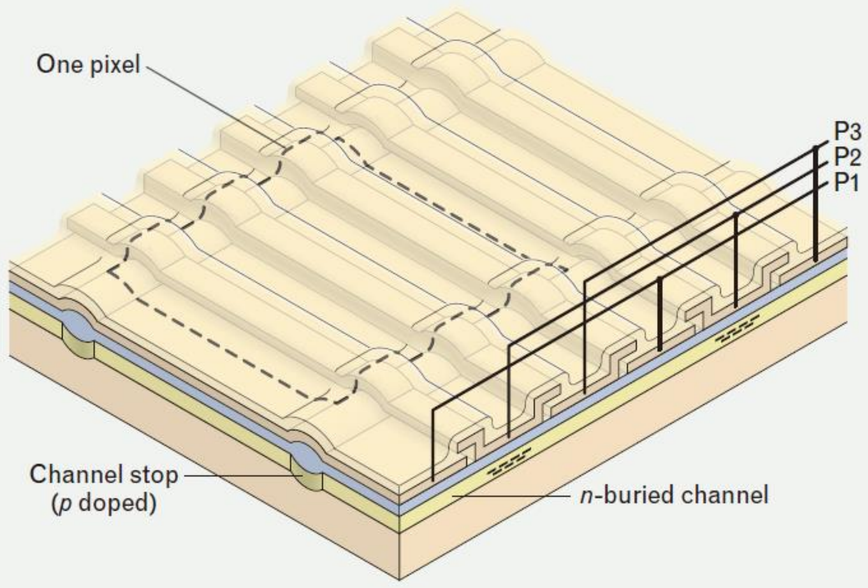

FIGURE B. Three-phase CCD showing the silicon substrate, doped layers comprising the buried channel and channel stops, gate and channel-stop dielectric layers, and the polysilicon gates.

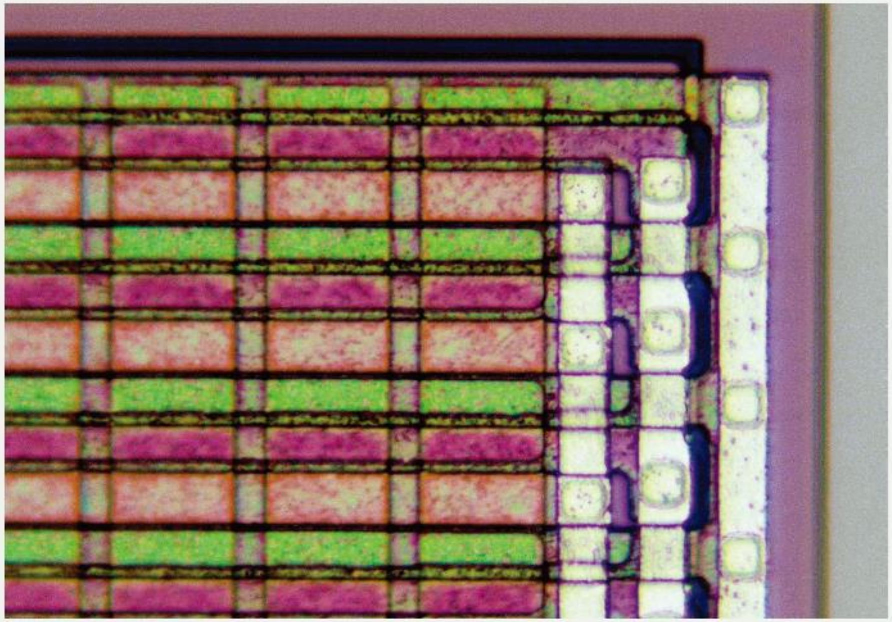

FIGURE C. The corner of a three-phase CCD imager, showing the narrow vertical channel stops, the three polysilicon gate levels, and the aluminum clock busses.

Burk et al. 2007

CCD : Different types of transfer

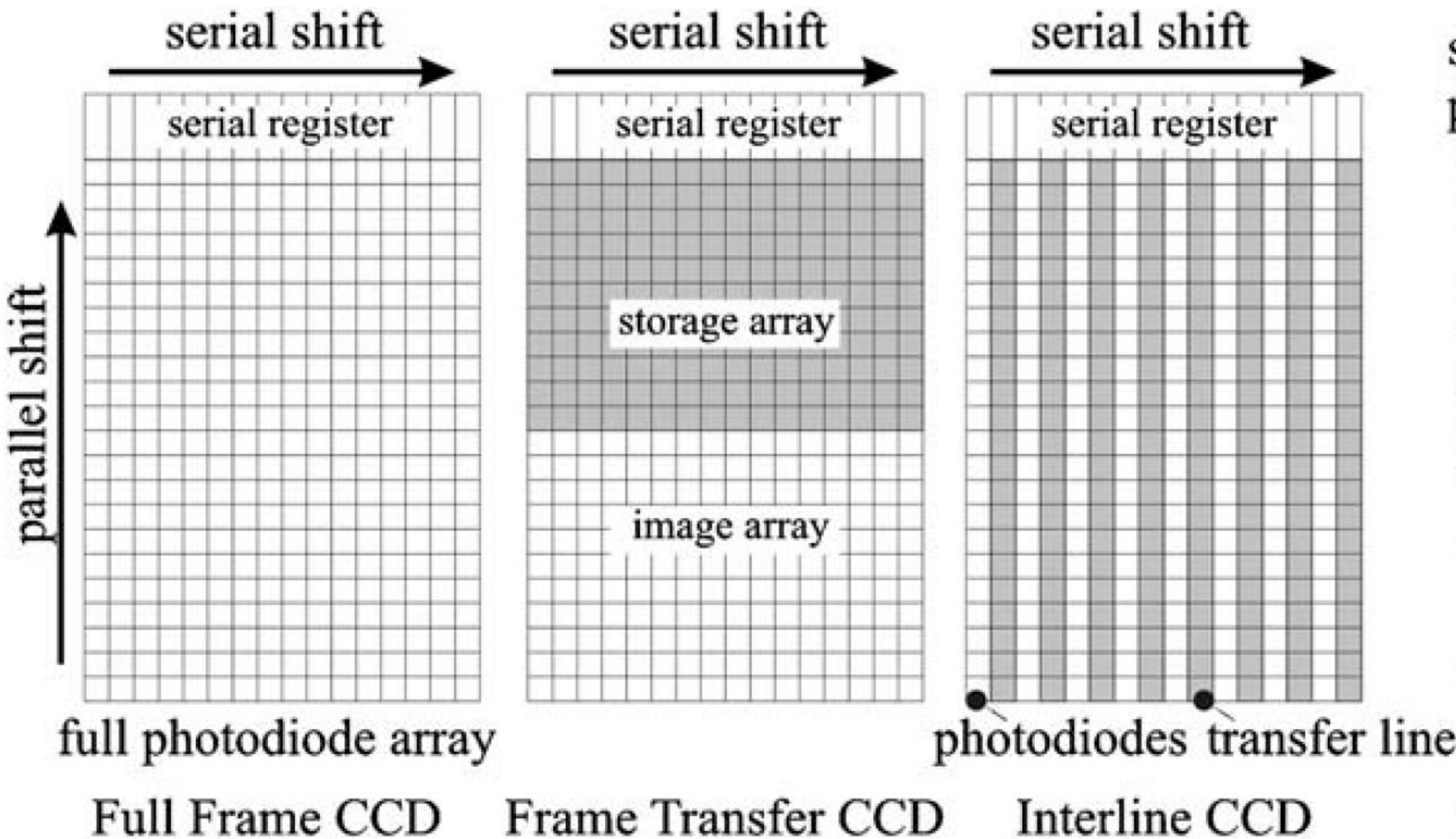

Sibarita 2005

Measure the number of electrons (I)

Noise: reset noise : correlated double sampling

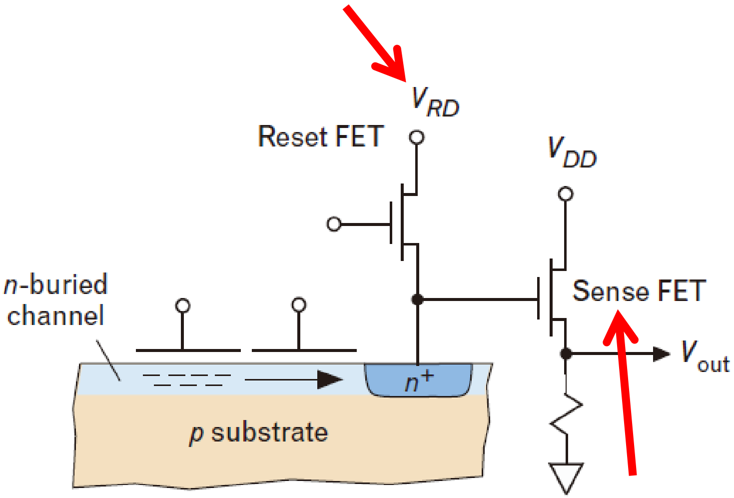

Noise: sensing noise

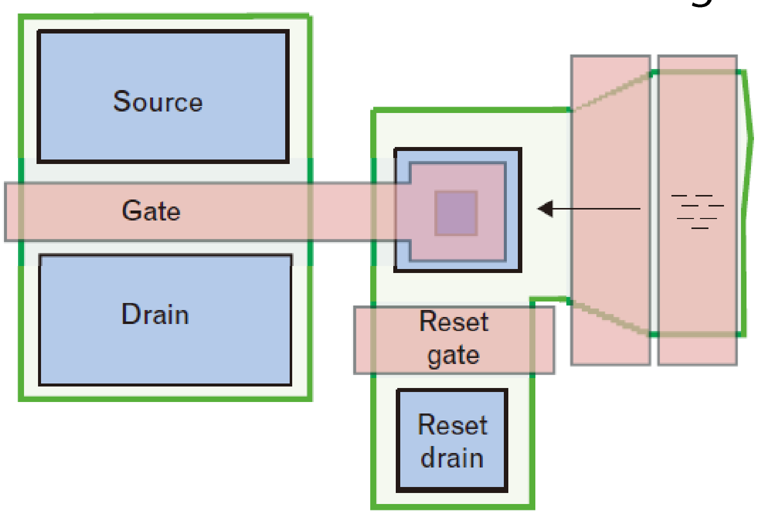

- Reset to VRD level
- N electrons makes change in the voltage level by

$$qN/C$$

C:capacitance, q:electron charge

- The output signal is proportional to N

$$V_{signal} = G\frac{qN}{C} = RN$$

G: source follower gain

- R is typically about 20uV/e
- Vout is amplified and converted to digital signal by AD converter.

Burk et al. 2007

IR array basic structure (1)

- Hybrid structure of IR array : different from CCD

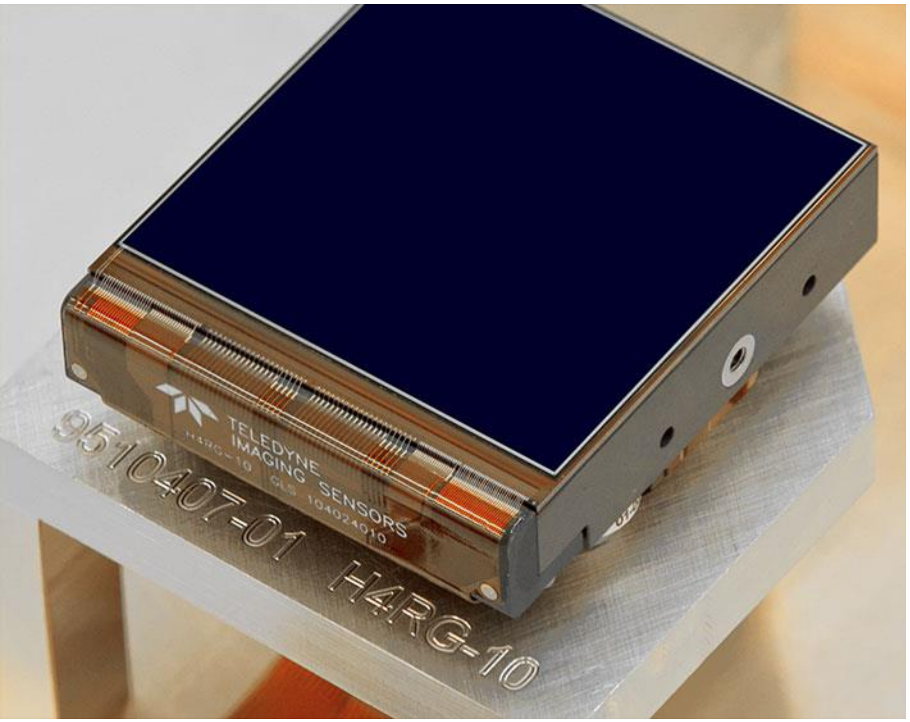

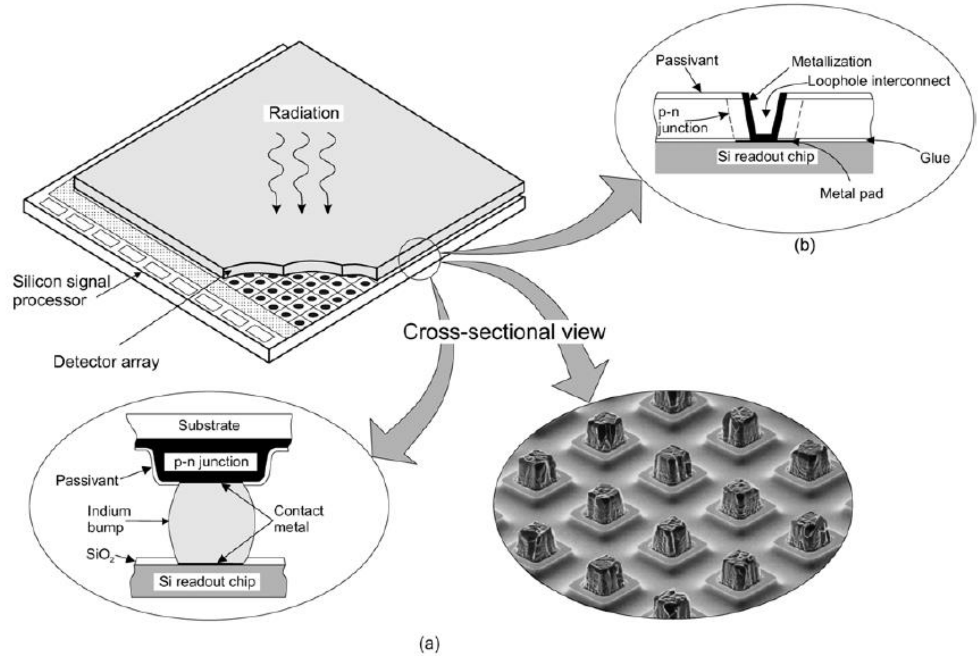

Figure 17. Hybrid IR FPA with independently optimized signal detection and readout: (*a*) indium bump technique and (*b*) loophole technique.

Teledyne Hawaii array : H4RG : 4Kx4K

Rogalski 2005

IR array basic structure (2)

- Readout integrated circuits (ROICs) inside the detector
- Non-destructive readout : measure the voltage level

MOSFET: transister

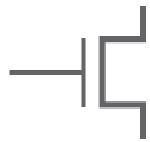

Figure 3

This figure shows a readout circuit—four cells of a detector array (the detectors are shown schematically as diodes). Signal is collected from the photodiode in the form of a current that deposits charge on the gate of transistor T_1 until it is judged time to measure the integrated level of charge. To read it out, power is applied to the row driver R_1 and, at the same time, to C_1. The transistors T_2, T_3, and T_4 conduct current as a result, and apply power to T_1 as well as connecting it to the output bus, which connects the signal to the output amplifier of the array (*lower left* in the figure) where it can be measured with an external circuit. There is now a choice. If one wants to continue integrating the signal, power is removed from C_1, and T_2, T_3, and T_4 turn off, removing power from T_1, so the pixel can continue to accumulate charge on its gate. Possibly, power would be applied to C_2 to read out the next pixel in the row of the array. In any case, these steps provide a nondestructive read of the upper left pixel, because they allowed determination of the level of detected charge without disturbing it. In the second case, one resets the collected charge and initiates a new integration. To do so, the reset line (below the row bus in the figure) is pulsed while T_2, T_3, and T_4 are still on, which sets the integrating node (the input to T_1) to the voltage V_R. Because the integrated charge is lost in this operation, and assuming one reads out T_1 before the reset, this operation has caused a destructive read. It is therefore possible to address each pixel in the array individually, read out the signal it has accumulated, and either continue through the array or reset the signal for a new integration. Figure from Rieke (2003), reproduced by permission of Cambridge University Press.

Rieke et al. 2007

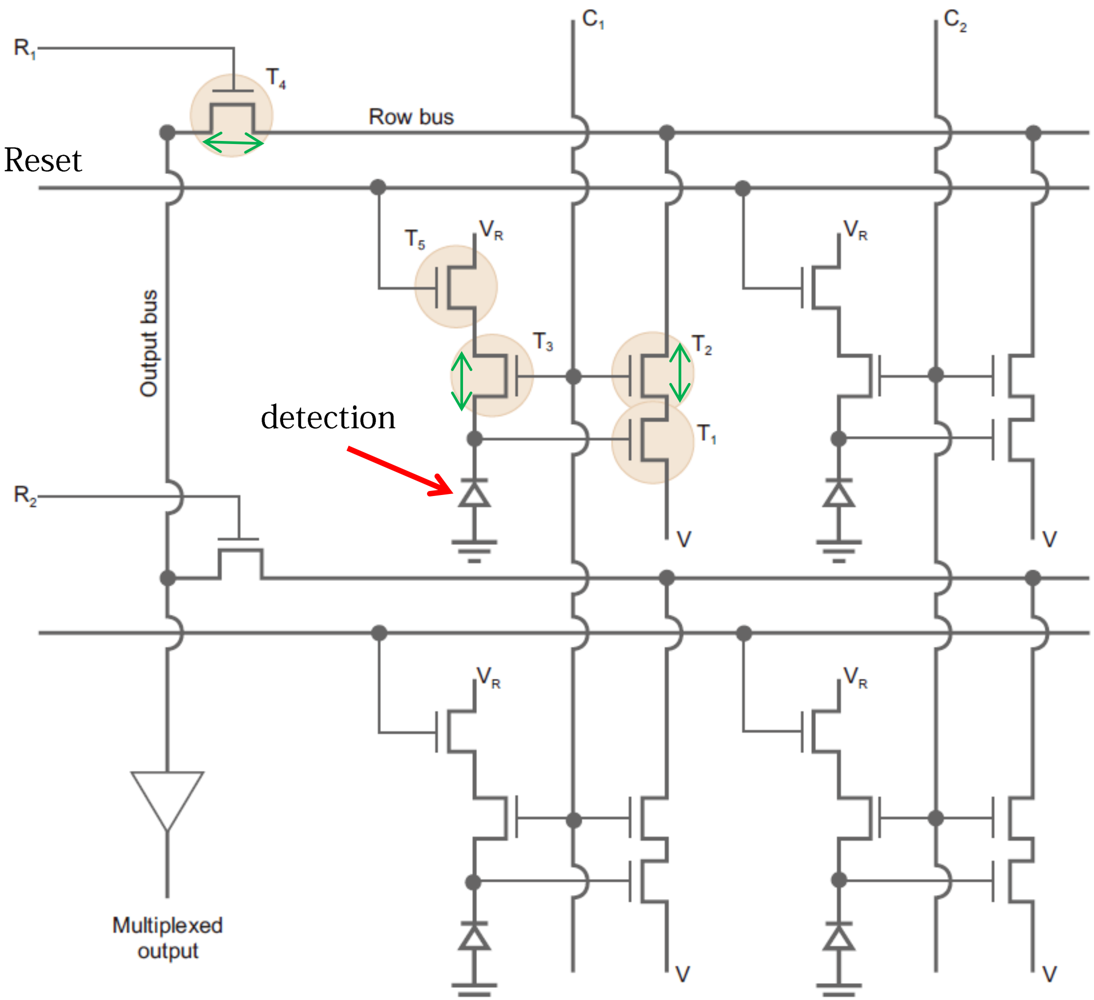

Merit of non-destructive readout

- Read-out can be made even during integration of light.

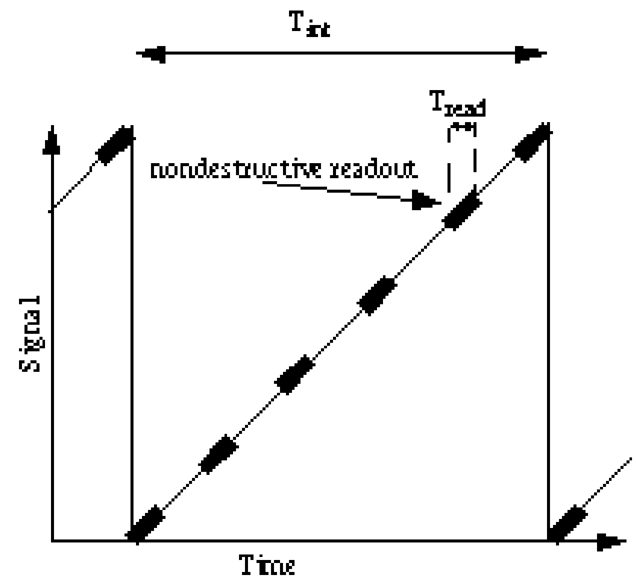

Figure 1 a: Follow up the ramp sampling. Nondestructive readouts are equidistantly distributed along the integration ramp. The slope of the integration ramp is calculated for each pixel by a least squares fit.

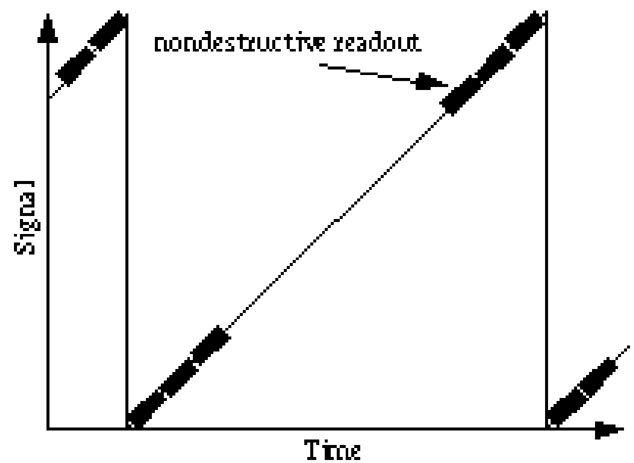

Figure 1 b: Fowler sampling. Nondestructive readouts are concentrated at the beginning and at the end of the integration ramp. The slope is calculated by averaging the slope of all Fowler pairs.

Finger et al.

CCD vs.(science)CMOS

- Each pixel has an amplifier and each pixel is addressed.

～CCDの読み出し方法～

CCDの構造

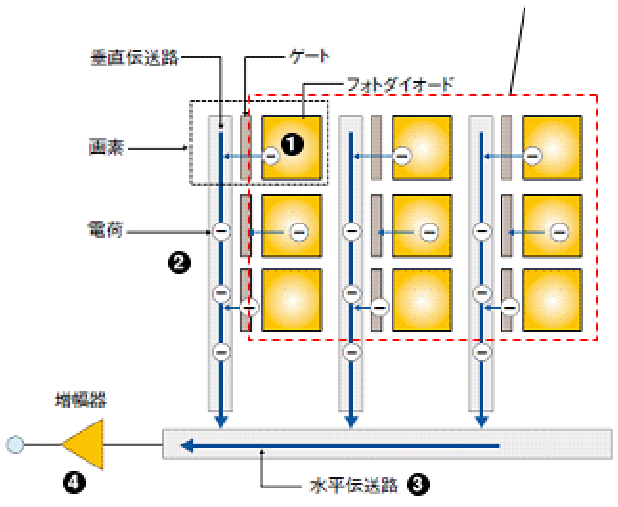

❶ 画素内のフォトダイオード（受光部）で光を受光し、電荷に変換して蓄積する。

❷ 全ての受光部に蓄積された電荷は、同時に垂直伝送路（垂直CCDレジスタ）に転送される（**全画素同時露光一括読み出し**）。

❸ 垂直伝送路を経由した電荷は、水平伝送路（水平CCDレジスタ）に転送される。

❹ 水平伝送路から転送されてきた電荷は、最後の増幅器で電荷から電圧に変換、増幅されてカメラ信号処理に送られる。

小型HDカムコーダーでは、常時全ての
水平・垂直レジスタでバケツリレーしているため
特殊な高電圧が必要、消費電力が大きく高速化に限界がある

～CMOSセンサーの読み出し方法～

CMOSセンサーの構造

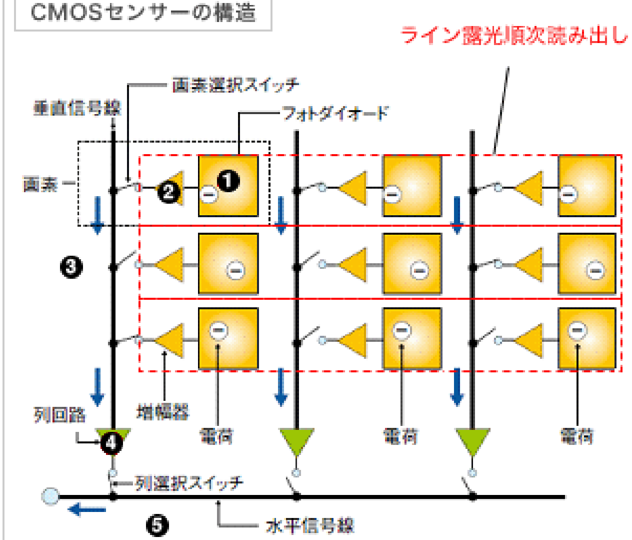

❶ 画素内のフォトダイオード（受光部）で光を受光し、電荷に変換して蓄積する。

❷ 蓄積された電荷は、画素内にある増幅器によって電圧に変換、増幅される。

❸ 増幅された電圧は、画素選択スイッチのON/OFFにより、ライン毎（行毎）に垂直信号線に転送される（**ライン露光順次読み出し**）。

❹ 垂直信号線毎に配置されている列回路（CDS回路）により、画素間にばらつきのあるノイズを除去し、一時的に保管する。

❺ 保管された電圧は、列選択スイッチのON/OFFにより水平信号線に送られる。

小型HDカムコーダーでは、読み出される
1行分の回路のみ動かせば良いので
低電圧な電源で構成、消費電力が低く高速化が容易

From sony.jp

Science CMOS : structure

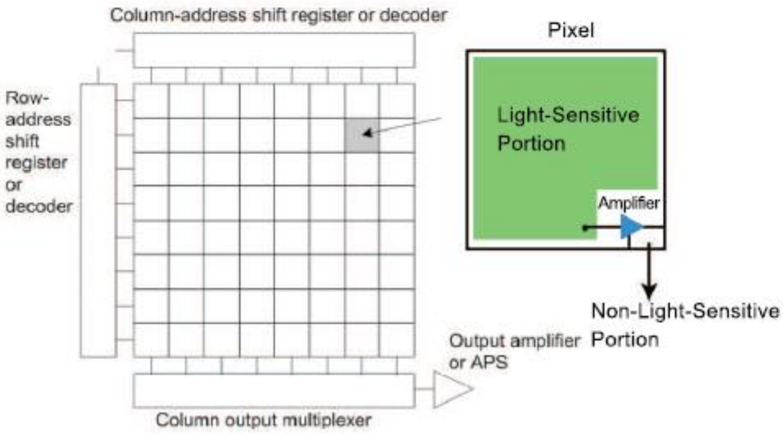

Qiu et al.

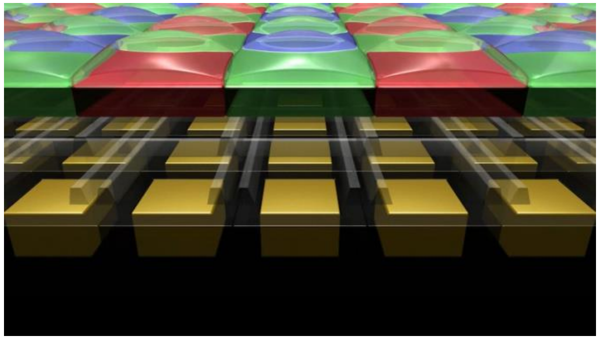

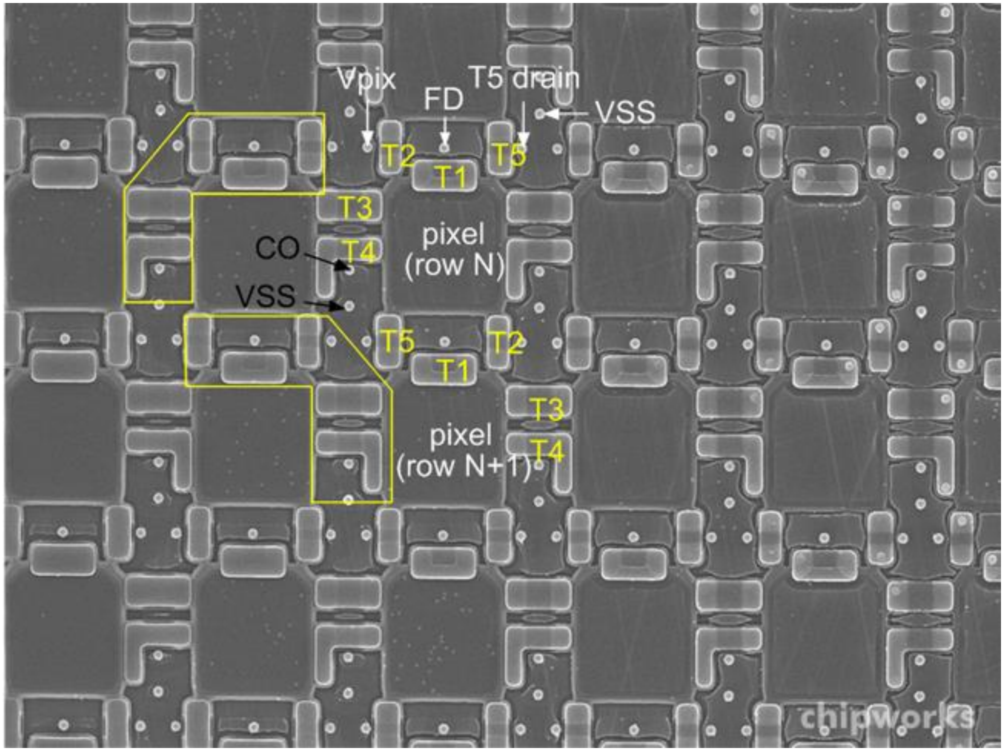

From chipworks.com

CCD : Parameters

- Quantum efficiency >90%
- Read-out speed ~ 24s (Subaru/FOCAS 2Kx4K CCD : <1MHz pixel)
- Linearity <1% typically
- Saturation level ~ 40,000 e- (Subaru/FOCAS CCD)
- Read-out noise ~ 4e- rms (Subaru/FOCAS CCD)
- Dark current (thermal electron) ~ 10e- / hour : (Subaru/HDS CCD)

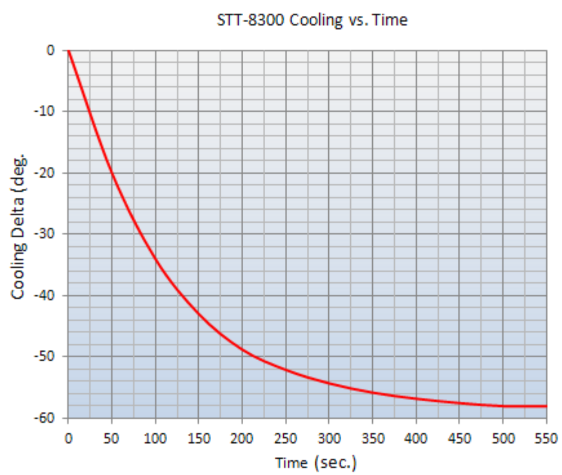

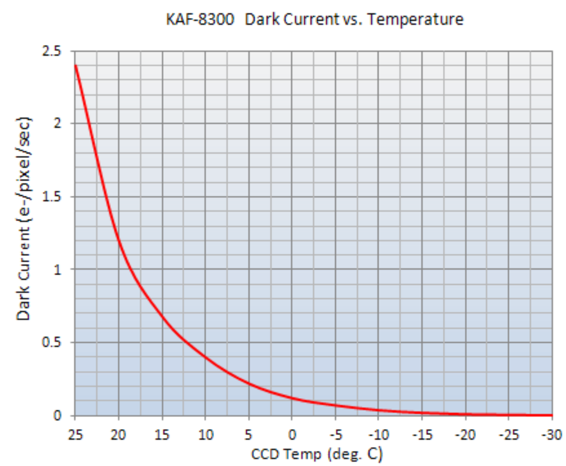

- Charge Transfer Efficiency (CTE) ~ 0.99999 = 0.9995 (1024 pixels)
(Hamamatsu CCD homepage) : Charge Transfer Inefficiency (CTI)

CCD : Read-out noise

- Read-out noise and read-out speed

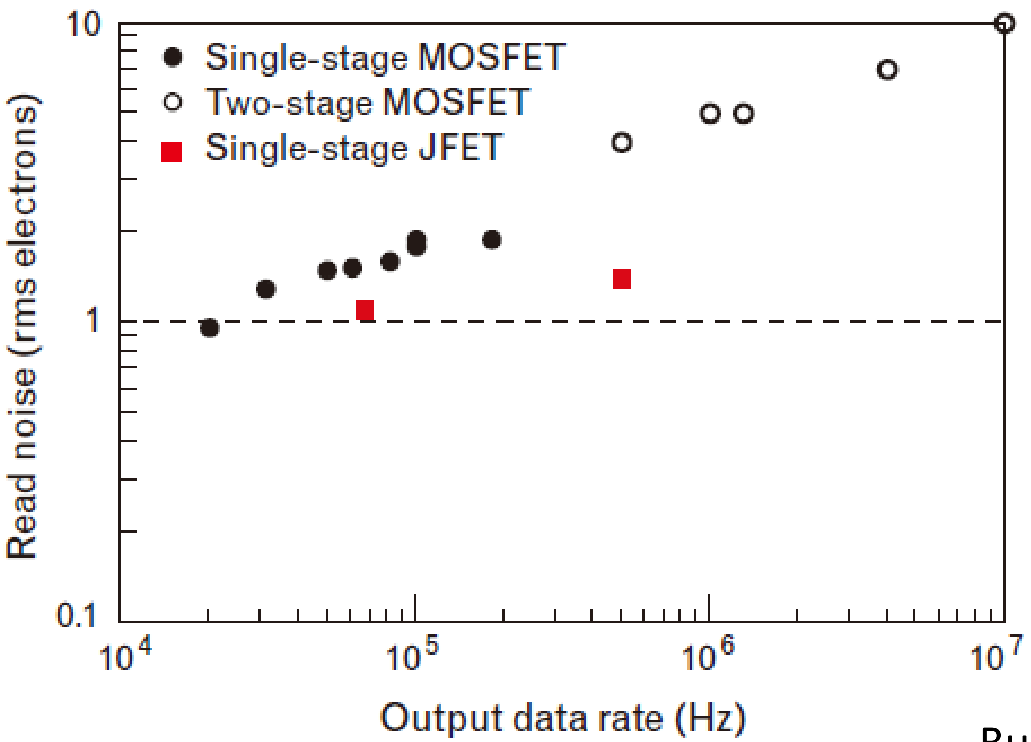

Burk et al. 2007

FIGURE 7. Summary of the best noise values obtained with Lincoln Laboratory CCDs. Included as red squares are preliminary results from the JFET version of the amplifier.

Science CMOS : Parameters (Andor Neo5.5 sCMOS)

- Quantum efficiency ~60-80%
  - Fill factor is not high, but with help of micro lens, high efficiency is acheived.

- Read-out speed ~ 30 fps (2560x2160, 200MHz pixel)
- Saturation level ~ 30,000 e-
- Read-out noise ~ 2.3 - 2.5e- rms
- Dark current ~ 25e- / hour @-40C
- Pixel size 6.5um (vs. 15um Hyper-Scam CCD, 24um EM-CCD:CCD60)
- Uniformity ?

Typical parameters of NIR arrays

- Noise, QE, number of pixel ：

Materials and Performance Levels for Detectors on the *Spitzer Space Telescope* and the *James Webb Space Telescope*

Array Type	Spectral Range (μm)	Pixel Count	Dark Current (e^-/s)	Temperature (K)	Noise (e^-)	Quantum Efficiency
***Spitzer* (2003)**						
InSb	2.8–5	131 072	0.5	15	6.8*	0.86
Si:As IBC	5–26	180 224	2.4	6	6.6*	0.55
Si:Sb IBC	14–38	32 768	<40	4	30*	0.25
Ge:Ga	51–106	1024	156	1.5	92*	0.18
Stressed Ge:Ga	140–174	40	500	1.5	280*	0.15
***JWST* (2011)**						
$Hg_{0.55}Cd_{0.45}Te$	0.6–2.3	46 137 344	<0.001	37	5†	0.95
$Hg_{0.70}Cd_{0.30}Te$	2.4–5	20 971 520	<0.001	37	5†	0.95
Si:As IBC	5–28	3 145 728	≪0.1	7	<19†	>0.7

*Read noise only, integrations <200 s. †Total noise, integrations 1000 s.

Richards 2005

CCD : thined back-side illuminated CCD

- Illuminating from back-side with thinning of the Silicon layer. Higher sensitivity in the short wavelength range.

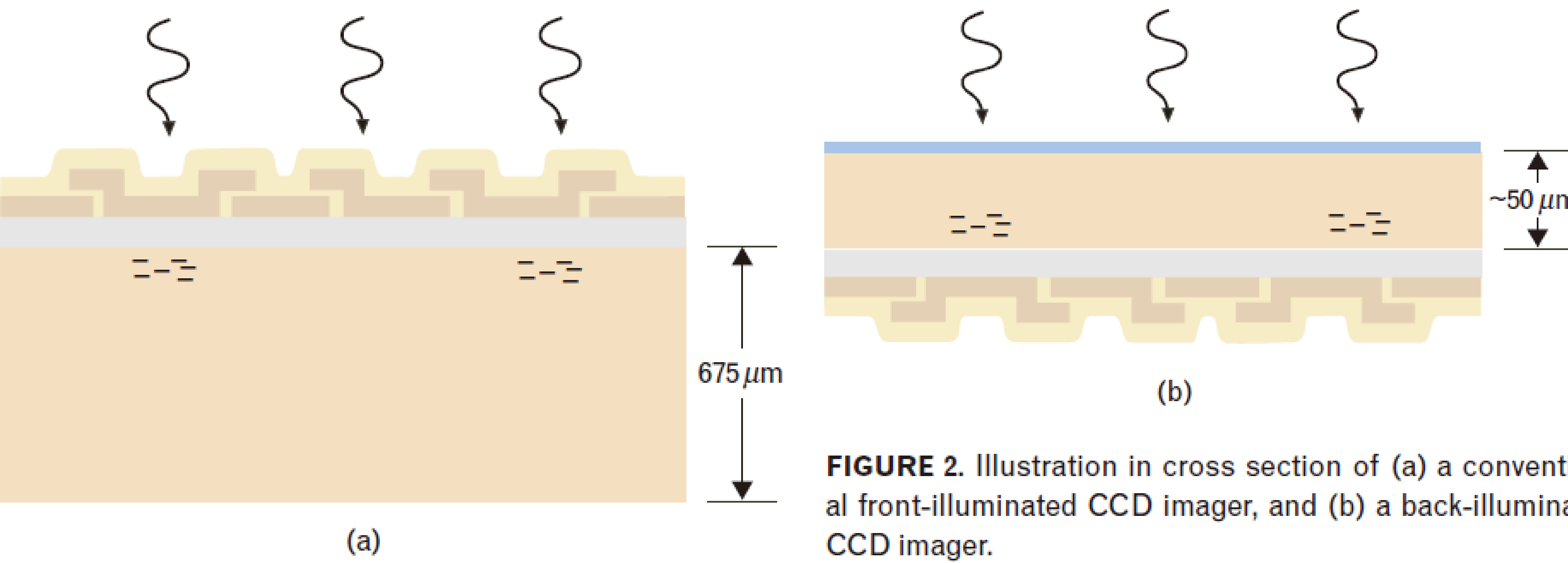

FIGURE 2. Illustration in cross section of (a) a conventional front-illuminated CCD imager, and (b) a back-illuminated CCD imager.

Burk et al. 2007

CCD : thined back-side illuminated CCD

- Illuminating from back-side with thinning of the Silicon layer. Higher sensitivity is achieved.

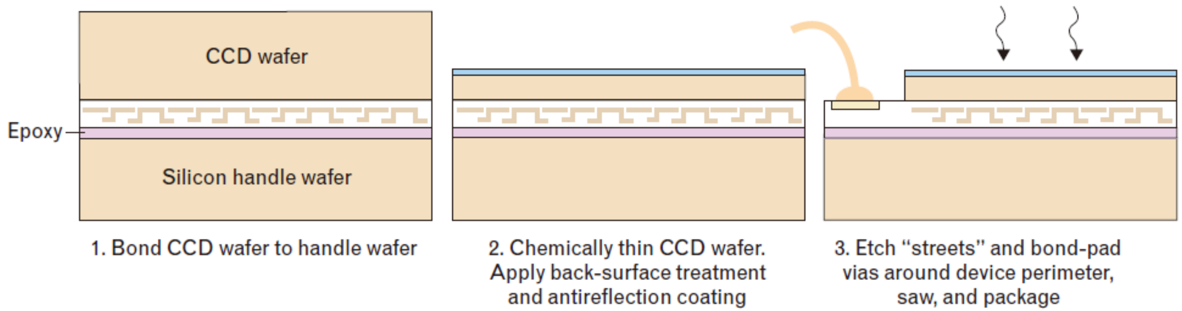

FIGURE 3. Processing steps in the fabrication of back-illuminated CCDs.

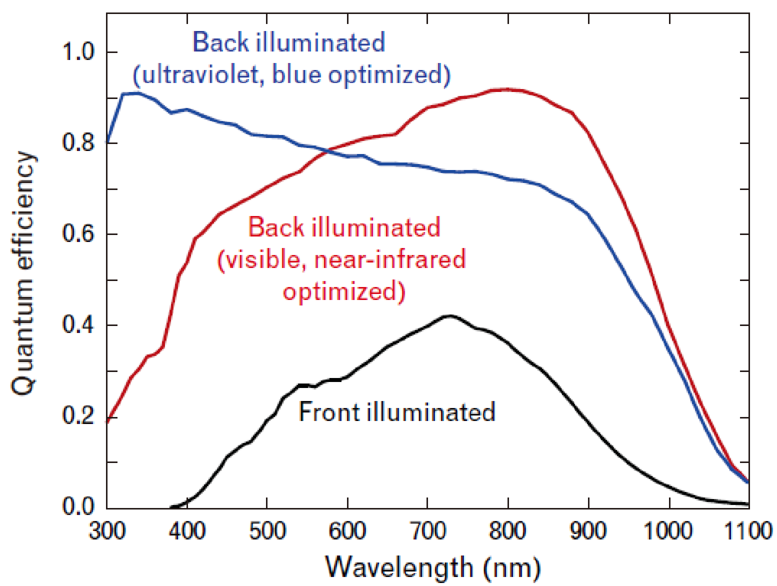

FIGURE 4. Quantum efficiencies of front-illuminated CCDs with back-illuminated CCDs optimized for short and long wavelengths.

Burk et al. 2007

Special CCD : Full-depletion CCD

- Thick depletion layer to make the quantum efficiency in red wavelength range (~90% at 900nm).
- Electron scattering size is proportional to the thickness of the depletion layer, sqrt(temperature), and 1/sqrt(Vbias) : scattering results in larger PSF.

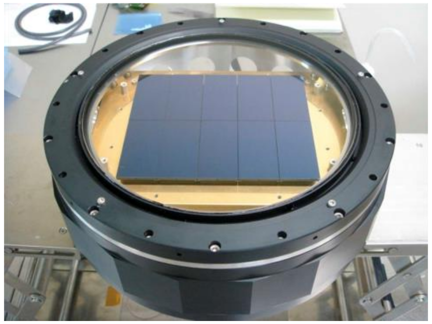

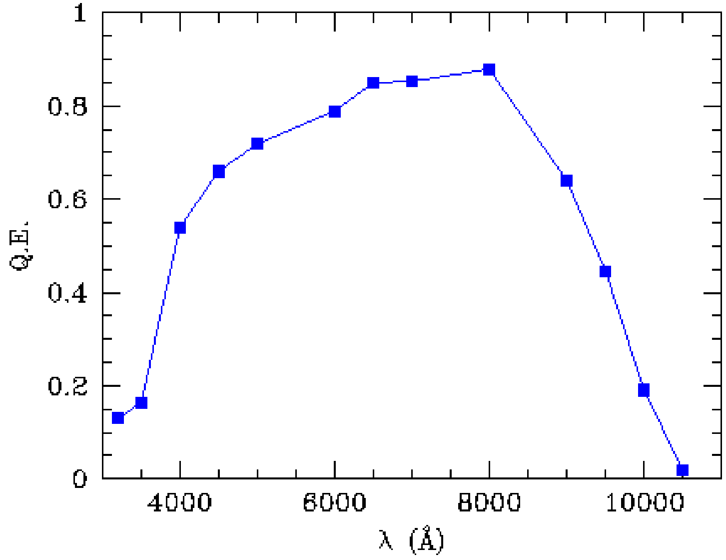

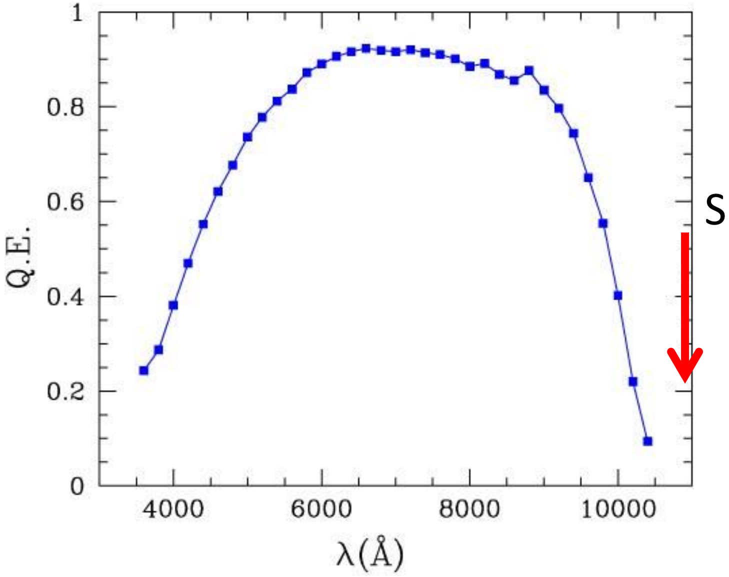

Special CCD : EM-CCD

- Low effective readout noise with electron multiplication.
- Pixel read out speed with >10MHz.

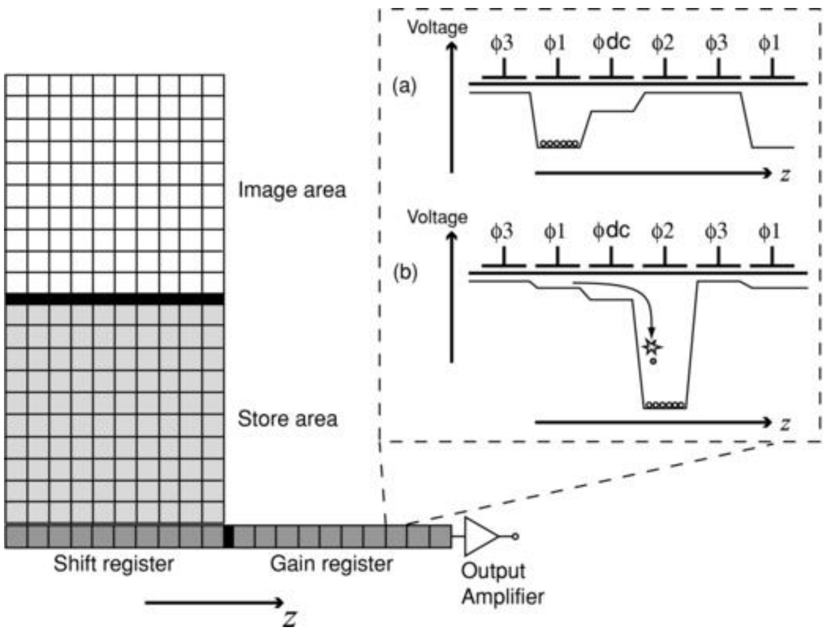

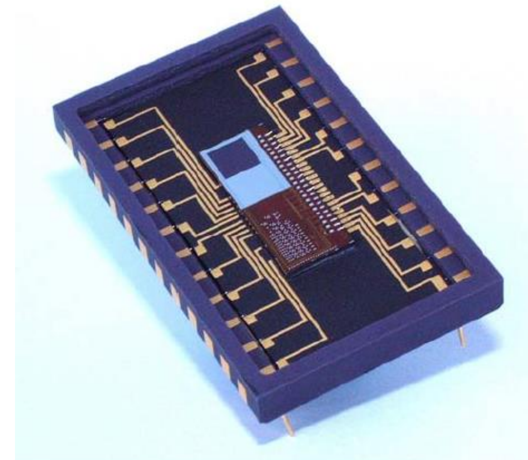

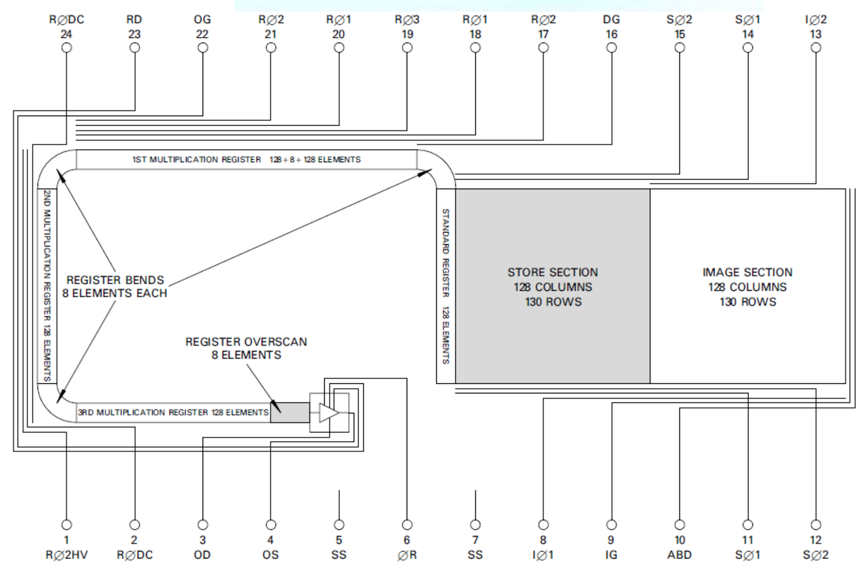

Special CCD : EM-CCD

- 4Kx4K EM-CCD 4fps

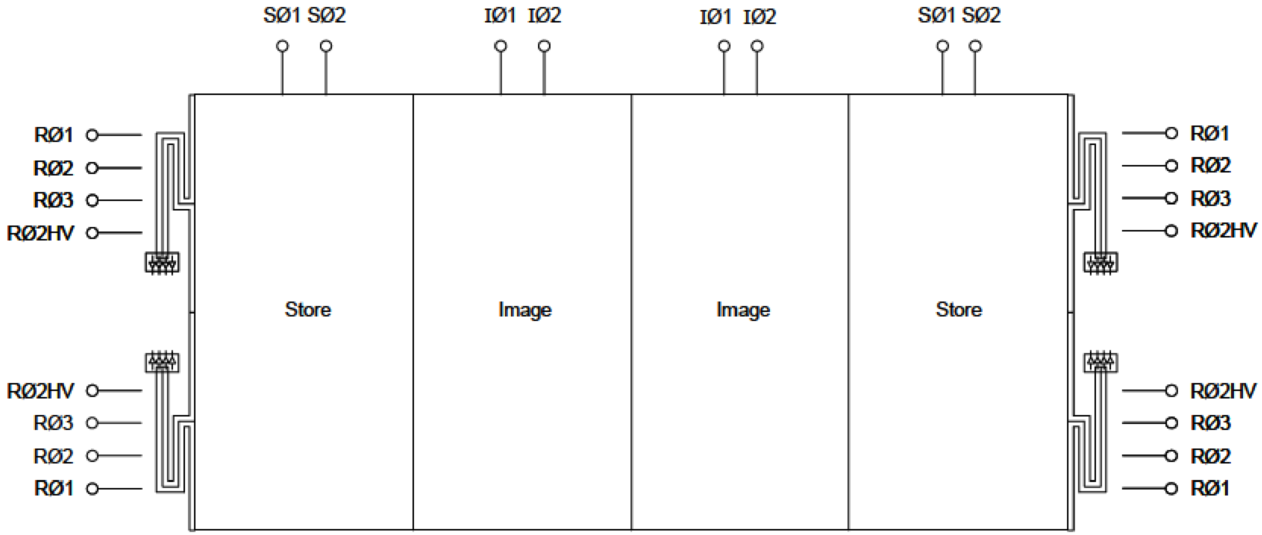

103 mm die length

Jorden SPIE

Special CCD : Orthogonal-Transfer-CCD

- Electrons in each pixel can move in both of the horizontal and vertical direction.

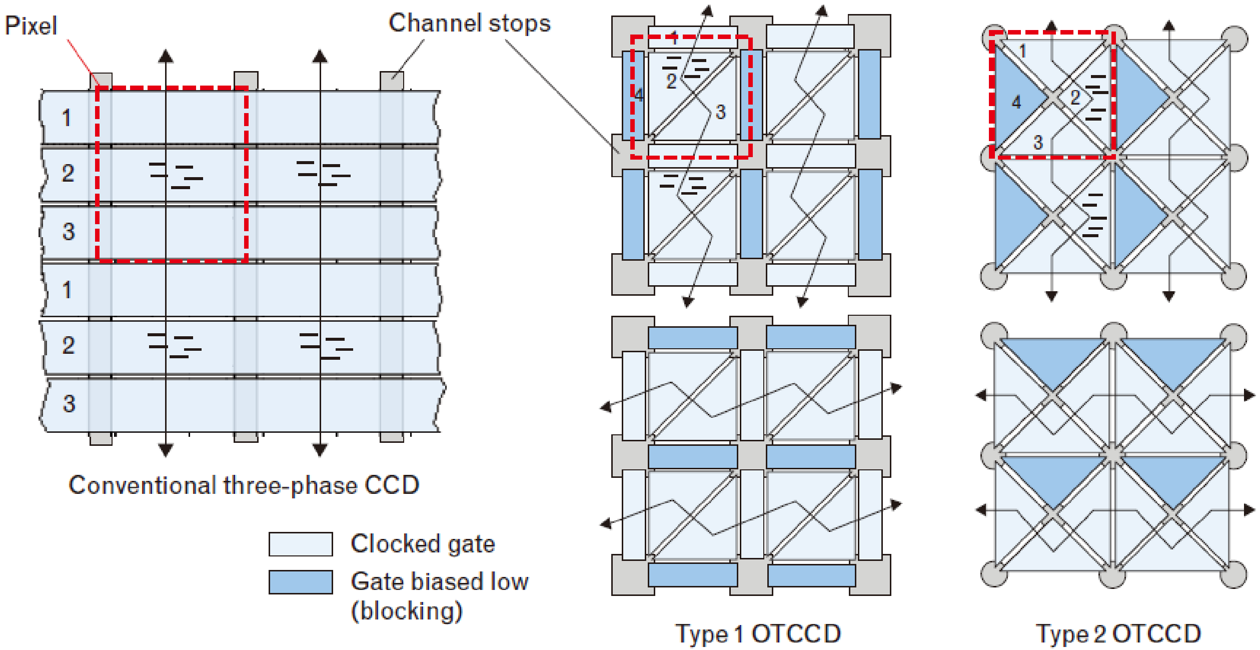

FIGURE 13. Depiction of the gate architecture and charge flow of a conventional three-phase CCD (left) and of two types of orthogonal transfer CCDs, or OTCCDs (right).

Burk et al. 2007

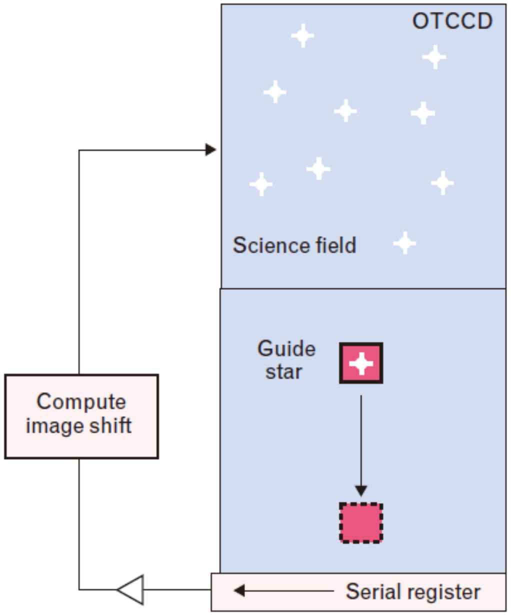

FIGURE 14. Depiction of the first use of an OTCCD for motion compensation in an astronomical application. The upper portion of the device has OTCCD pixels that are shifted to track the random image motion arising from atmospheric wavefront distortion. The lower portion of the device is operated independently as a star tracker at frame rates sufficient to track the image motion and provide feedback to shift the OTCCD pixels.